Extreme Mechanics Letters 35 (2020) 100622

Contents lists available at ScienceDirect

Extreme Mechanics Letters

journal homepage: www.elsevier.com/locate/eml

A discrete differential geometry-based approach to numerical simulation of Timoshenko beam

Xuanhe Li[1], Weicheng Huang[1], M. Khalid Jawed *

Department of Mechanical and Aerospace Engineering, University of California, Los Angeles, CA 90095, United States

ARTICLE INFO

Article history:
Received 30 October 2019
Received in revised form 18 December 2019
Accepted 21 December 2019
Available online 30 December 2019

Keywords:
Timoshenko beam
Numerical simulation
Elasticity

ABSTRACT

We report a discrete differential geometry-based numerical method for the simulation of geometrically nonlinear dynamics of thick beam — known as Timoshenko beam. Our numerical framework discretizes the beam into a number nodes and uses the degrees of freedom of each node – position and rotation angle – to construct discrete elastic energies. Equations of motion resulting from balance of forces are formulated at each degree of freedom. These equations are integrated using a second order, implicit Newmark-beta time marching scheme. We find that the structural rigidity and natural frequency computed in Timoshenko beam framework are always lower than the one obtained using Euler–Bernoulli beam method for both naturally straight and curved beams. For quantitative comparison, we analytically solve the Euler–Lagrange equations using both Euler–Bernoulli and Timoshenko beam theories for a number of examples. A good match between the analytical solution and the numerical results in the geometrically linear regime indicates the correctness of our discrete model. The simulation can seamlessly handle geometrically nonlinear deformation that is often not amenable to an analytical approach.

1. Introduction

Beams, as one of the most important structural components for bearing external loading, have been widely used in both macro scale (e.g. composite laminates [1–3]) and micro/nano systems (e.g. sensors [4–7] and actuators [8,9]). Analysis of beam structures dates back to the 18th century when Euler and Bernoulli proposed a simplified one dimensional model that accounts for the normal stress and related inertia but disregards rotational inertia and transverse shear. However, neglecting this shear deformation can lead to intolerant errors if length to width ratio of the beam is large. Rayleigh proposed an improved theory that involved the rotational inertia of the cross section [10]. Later, in 1921, Timoshenko introduced both shear stiffness and rotary inertia on the basis of Euler–Bernoulli model [11,12], and since then, this model has been associated with his name. A comprehensive overview of these beam theories and a detailed comparison of their applications in structural mechanics community can be found in Refs. [13,14].

In the computational mechanics community, numerical simulation of Timoshenko beam is typically performed by the Finite Element Method (FEM) [15–18] and the Boundary Element Method [19–24]. A different type of numerical frameworks based on Discrete Differential Geometry (DDG) [25] is popular in the computer graphics community for simulation of slender structures, e.g. hairs and clothes, due to computational efficiency and the ability to include geometrically nonlinear deformation, contact, and collision. The DDG approach starts with discretization of the smooth system into a mass–spring-type system, while preserving the key geometric structures [25]. Prior DDG-based numerical frameworks were surprisingly successful in simulating thin elastic structures, e.g. rods [26–29], ribbons [30], viscous threads [28,31], plates/shells [32–34], and gridshell/cosserat net [35–37]. One DDG-based simulation algorithm in particular – the Discrete Elastic Rods (DER) method [27,28,38] for simulation of geometrically nonlinear dynamics of thin elastic rods – has been embraced by the mechanics community. Excellent agreement has been found between DER-based simulations and physical experiments [39–42]. However, previous works with DER employ Kirchhoff's rod model [43] and this model, in the planar (two-dimensional) case, shares the same assumption with Euler–Bernoulli beam model [44]: the structure is unshearable. Several structural components in a variety of applications, e.g. sandwich composite beam [45], soft robotics [46], and soft electronics [47], are usually manufactured with shearable thick beams [44]. The shear strain in elastic filaments is increasingly recognized as an important effect, e.g. in case of simulation of musculoskeletal architectures [48]. This raises the need for numerical methods that are able to take the shear strain and rotational inertial into

* Corresponding author.
E-mail address: khalidjm@seas.ucla.edu (M.K. Jawed).
[1] X.L. and W.H. contributed equally to this work.

https://doi.org/10.1016/j.eml.2019.100622
2352-4316/

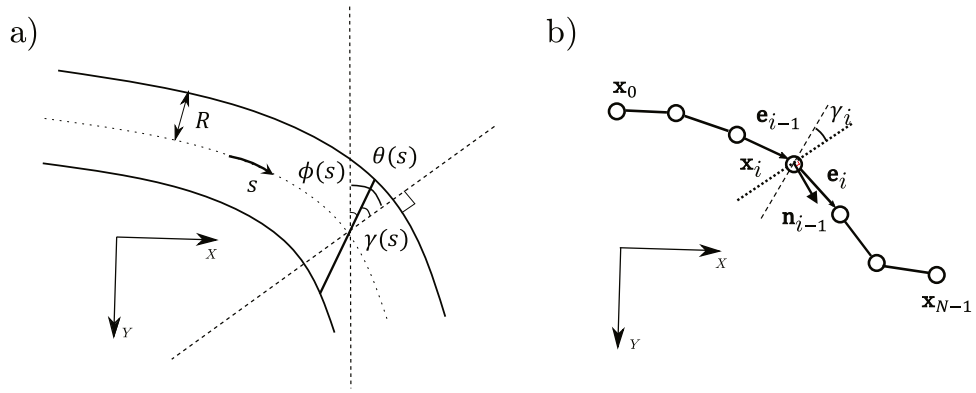

Fig. 1. (a) Schematic diagram of Timoshenko beam in continuous case. (b) Schematic and relevant notations for Discrete Elastic Timoshenko Beam Simulation.

account, as well as include the geometric nonlinearity during the deformation process. Relevant works that consider shear-induced effects in filamentary structures include a numerical method proposed by Gazzola et al. based on Cosserat theory of stretchable and shearable filaments [44].

Here, we present a DDG-based implementation of Timoshenko beam simulation for both static and dynamic behaviors under arbitrary boundary conditions and external loading. The thick beam is divided into a number of nodes along the centerline; the positions of these nodes and the shear strains therein are the degrees of freedom of the beam. Discrete elastic energies at each node are formulated in terms of the degrees of freedom. These elastic energies are then used to derive the equations of motion at each degree of freedom. To avoid the artificial energy dissipation, a second order, symplectic Newmark-beta time marching scheme [49,50] is used to integrate the equations and simulate the structural dynamics of Timoshenko beam. Three examples – static deformation of a naturally straight beam, dynamic frequency of a naturally straight beam, and the static deformation of a naturally curved beam – are simulated using the original DER method and the newly introduced Timoshenko beam simulator. The results are compared to underline the significance of shear deformation and rotational inertia. In parallel with numerical investigation, we analytically solve the Euler–Lagrange equations obtained from functional variation in the linear regime and compare the analytical solutions with numerical data to check the accuracy of our simulator. A good match between numerical simulation and analytical results at small deflection indicates the correctness of the numerical scheme. While the analytical solutions do not hold for geometrically nonlinear deformation, the DDG-based simulation can robustly capture such deformation.

Our paper is organized as follows. In Section 2, we start with the continuous energy functional of both Euler–Bernoulli and Timoshenko beam and then discuss their discrete representation. Next, in Section 3, we show both numerical data and analytical results for several demonstrative examples. Finally, conclusive remarks and future research directions are presented in Section 4.

2. Methods

In this section, We discuss the numerical framework of Timoshenko beam simulation. We first briefly review the classical Euler–Bernoulli beam theory and Timoshenko beam theory, then followed by a Discrete Differential Geometry (DDG) based discretization of continuous model, i.e. the formulations of elastic energies, elastic forces, and the time marching procedure of the solver in a discrete format.

2.1. Beam theory in continuous case

We start with the classical Euler–Bernoulli beam theory. For a beam made with linear elastic material that undergoes small deflection, its total elastic potential and kinetic energies are [10]

$$E_{\text{Euler}} = \frac{1}{2}\int_0^L EA(\epsilon)^2 ds + \frac{1}{2}\int_0^L EI(w'')^2 ds \tag{1a}$$

$$T_{\text{Euler}} = \frac{1}{2}\int_0^L \rho A(\dot{w})^2 ds + \frac{1}{2}\int_0^L \rho I(\dot{w}')^2 ds, \tag{1b}$$

where E is the Young's modulus, A is the cross sectional area, I is the second moment of inertia of the cross section, ρ is the material density, L is the arclength, s is the arclength parameter, w is the deflection, and ϵ is the axial strain. Here, we follow the convention of using the overdot (and prime) to represent the time derivative (and space gradient with respect to s). Note that $w' \approx \theta$ (and $w'' \approx \kappa$) is the rotation angle (and curvature) of the beam centerline.

In Euler–Bernoulli beam theory, we model the cross section of a deformed beam as a rigid plane that always remains perpendicular to its centerline, such that the normal strain energy is predominant and we can ignore the elastic potential energy related to shear strains. This formulation is accurate when the ratio between length, L, and thickness, D, of the beam is large, i.e. $L/D \gg 1$. However, when it comes to a thick beam, such simplification could lead to unacceptable errors and a modification to the energy models is necessary. Timoshenko first proposed a new beam theory in the early 20th century [11,12]. In this model, the rotation of the cross section is independent of beam deflection and the shear deformation is taken into account. In Fig. 1(a), we show the rotation of the beam cross section relative to its centerline, and this rotation angle is defined as $\gamma(s)$. In fact, $\gamma(s)$ is the shear strain of the beam that is assumed to be zero in the Euler–Bernoulli beam theory. By releasing the constraints on the rotation of cross section discussed above, the total elastic potential energies as well as the kinetic energy in Timoshenko beam theory are given by [11,12]

$$E_{\text{Timo}} = \frac{1}{2}\int_0^L EA(\epsilon)^2 ds + \frac{1}{2}\int_0^L EI(\kappa - \gamma')^2 ds + \frac{1}{2}kGA\int_0^L \gamma^2 ds \tag{2a}$$

$$T_{\text{Timo}} = \frac{1}{2}\int_0^L \rho A(\dot{w})^2 ds + \frac{1}{2}\int_0^L \rho I(\dot{w}' - \dot{\gamma})^2 ds, \tag{2b}$$

where κ is the curvature of beam centerline, G is the shear modulus, and k is the correction factor in Timoshenko's theory. This factor can be determined on the basis of the geometry of the cross section. In this paper, we choose $k = 3/4$ for circular

cross section. Note that if we replace κ by w'', Eq. (2) reduces to the standard linear Timoshenko beam model and describes the deformation of thick beam in geometrically linear regime.

The Euler–Lagrange equations describing the dynamics of the system are

$$\frac{\partial \mathbf{L}}{\partial \mathbf{q}} - \frac{d}{dt}\frac{\partial \mathbf{L}}{\partial \dot{\mathbf{q}}} = \mathbf{0}, \tag{3}$$

where $\mathbf{L} = T - E$ is the Lagrangian and $\mathbf{q}$ is the generalized degrees of freedom. If the external force is nonzero, we can add this term on the right side of the equation.

2.2. Discrete model

Analytically solving the Euler–Lagrange equations in Eq. (3) is not easy, especially when geometric nonlinearity comes into play. Inspired by the DER method, we introduce here the model behind the Discrete Elastic Timoshenko Beam method simulation of thick beams under large deflection. In the discrete setting shown in Fig. 1(b), we discretize the beam centerline into N nodes, $[\mathbf{x}_0, \mathbf{x}_1, \ldots, \mathbf{x}_{N-1}]^T$, that correspond to $N-1$ edge vectors, $[\mathbf{e}_0, \mathbf{e}_1, \ldots, \mathbf{e}_{N-2}]^T$, where $\mathbf{e}_i = \mathbf{x}_{i+1} - \mathbf{x}_i$. Hereafter, superscript T denotes the transposition operation. Besides the nodal positions, $\mathbf{x}_i \equiv [x_i, y_i]^T$, we introduce another degree of freedom, γ_i, per node that denotes the rotation angle of the beam cross section at the ith node. Overall, the method requires a $3N$-sized degree of freedom vector,

$$\mathbf{q} = [\mathbf{x}_0, \gamma_0, \mathbf{x}_1, \gamma_1, \ldots, \mathbf{x}_{N-1}, \gamma_{N-1}]^T. \tag{4}$$

Next, we formulate the discrete elastic and kinetic energy in terms of the degrees of freedom of the discrete beam. We model the Timoshenko's beam as a mass–spring system with a lumped mass and shear strain at each node, such that the associated stretching, bending, shearing, and kinetic energies are

$$E_{\text{stretching}} = \frac{1}{2}EA\sum_{i=0}^{N-2}(\epsilon_i)^2\|\bar{\mathbf{e}}_i\|, \tag{5a}$$

$$E_{\text{bending}} = \frac{1}{2}EI\sum_{i=1}^{N-2}(\kappa_i - \bar{\kappa}_i - \frac{\gamma_i - \gamma_{i-1}}{\Delta l_i})^2\Delta l_i, \tag{5b}$$

$$E_{\text{shearing}} = \frac{1}{2}kGA\sum_{i=1}^{N-2}(\gamma_i)^2\Delta l_i, \text{ and} \tag{5c}$$

$$T_{\text{kinetic}} = \frac{1}{2}\rho A\sum_{i=0}^{N-1}(\dot{\mathbf{x}}_i)^2\Delta l_i + \frac{1}{2}\rho I\sum_{i=0}^{N-1}(\dot{\gamma}_i)^2\Delta l_i, \tag{5d}$$

where $\epsilon_i = \|\mathbf{e}_i\|/\|\bar{\mathbf{e}}_i\| - 1$ is the axial strain associated with the ith edge, κ_i is the curvature of the ith node ($\bar{\kappa}_i$ is its undeformed curvature), $\|\bar{\mathbf{e}}_i\|$ is the Euclidean length of the ith edge in undeformed configuration, and $\Delta l_i = (\|\bar{\mathbf{e}}_{i-1}\| + \|\bar{\mathbf{e}}_i\|)/2$ is the Voronoi length of the ith node [27,28,38]. The curvature is obtained from the misalignment between two consecutive edge segments such that $\kappa_i = 2\tan(\phi_i/2)/\Delta L_i$, where ϕ_i is the angle between $\mathbf{e}_i$ and $\mathbf{e}_{i-1}$. Details of the energy discretization can be found in Appendix A.

By using variational principle, the discrete equations of motion (similar to Euler–Lagrange equations in Eq. (3)) for the beam system are

$$\mathbb{M}\ddot{\mathbf{q}} - \mathbf{F}^{\text{int}} = \mathbf{F}^{\text{ext}}, \tag{6}$$

where $\mathbb{M}$ is the diagonal mass matrix (we ignore the non-diagonal terms representing the inertial coupling between $\mathbf{x}_i$ and γ_i), $\mathbf{F}^{\text{int}} = -\nabla(E_{\text{stretching}} + E_{\text{bending}} + E_{\text{shearing}})$ is the internal elastic force vector, and $\mathbf{F}^{\text{ext}}$ is the external force vector. We use a second order, implicit Newmark-beta time marching scheme to numerically integrate the equations of motion from time step t_k to $t_{k+1} = t_k + h$ (h is the time step size) [49,50],

$$\mathbb{M}\Delta\mathbf{q}_{k+1} - h\mathbb{M}\dot{\mathbf{q}}_k - \frac{h^2}{4}\left(\mathbf{F}^{\text{int}}_{k+1} + \mathbf{F}^{\text{ext}}_{k+1} + \mathbf{F}^{\text{int}}_{k} + \mathbf{F}^{\text{ext}}_{k}\right) = \mathbf{0} \tag{7a}$$

$$\mathbf{q}_{k+1} = \mathbf{q}_k + \Delta\mathbf{q}_{k+1} \tag{7b}$$

$$\dot{\mathbf{q}}_{k+1} = \frac{2}{h}\Delta\mathbf{q}_{k+1} - \dot{\mathbf{q}}_k, \tag{7c}$$

where the subscript $k+1$ (and k) denotes the evaluation of the quantity at time t_{k+1} (and t_k). The Jacobian associated with Eq. (7) is necessary for Newton's iteration and can be expressed as

$$\mathbb{J} = \mathbb{M} - \frac{h^2}{4}\nabla(\mathbf{F}^{\text{int}} + \mathbf{F}^{\text{ext}}), \tag{8}$$

We used a symbolic computing environment (Matlab) to obtain the expressions for the Hessian matrix in our programming implementation. If the gradient of the external force vector, $\nabla\mathbf{F}^{\text{ext}}$, cannot be analytically evaluated, this term is often neglected, i.e. external forces are treated explicitly. Importantly, the Jacobian $\mathbb{J}$ is a banded matrix and the time complexity of this algorithm is $O(N)$ [28]. Notice that, if the shear strains, γ_i, are constrained to zero, the above discrete Timoshenko beam simulation reduces to the planar DER method based on geometrically nonlinear formulation of Euler–Bernoulli beam theory.

3. Results

In this section, we use the discrete model discussed above to investigate the static and dynamic behaviors of both Euler–Bernoulli beam (by standard DER method) and Timoshenko beam (by the newly introduced Discrete Timoshenko Beam framework). Also, for comparison, we analytically solve the Euler–Lagrange equations of Euler–Bernoulli and Timoshenko beams in some cases, and theoretical results are displayed to prove the correctness and accuracy of our numerical model. Details of the analytical solution can be found in Appendix B. A convergence study on the discretization along time and space is presented in Appendix C.

3.1. Static deformation of simply supported and clamped beams

The first example involves the static deformation of a simply supported beam in Fig. 2(a1) and a clamped-free beam in Fig. 2(a2). The physical parameters in this example are: beam length $L = 1.0$ m, diameter of circular cross section $D \equiv 2R = 0.2$ m, Young's modulus $E = 10$ MPa, and shear modulus $G = E/3k$ (with Poisson's ratio $\nu = 1/8$), where $k = 3/4$ for circular cross section. The number of nodes is $N = 100$ and the time step size is $h = 1$ ms. To achieve the final static configuration, we applied a small damping force, $\mathbf{F}^{\text{ext}} = -\mu\dot{\mathbf{q}}$ where μ is the viscous damping coefficient, in Eq. (7). Otherwise, in the absence of energy dissipation, the beam will vibrate forever under gravity.

In Fig. 2(a1–a2), we show a beam under uniform load, p, with two different boundary conditions: (a1) simply supported boundary conditions (with $x_0 = 0$; $y_0 = 0$; $y_{N-1} = 0$); and (2) clamped-free boundary conditions (with $x_0 = 0$; $y_0 = 0$; $x_1 = \|\bar{\mathbf{e}}_0\|$; $y_1 = 0$). Fig. 2(b1–b2) present the deformed shapes of the simply supported beam and the clamped-free beam, using two different numerical methods: original DER method (dash-dotted line) and Discrete Timoshenko Beam framework (solid line). The value of the load is $\bar{p} = 25.5$ for the simply supported beam and $\bar{p} = 2.6$ for the clamped-free beam We can observe that, under the same loading, the deflection of Timoshenko beam is larger than that of Euler beam. The physical interpretation is:

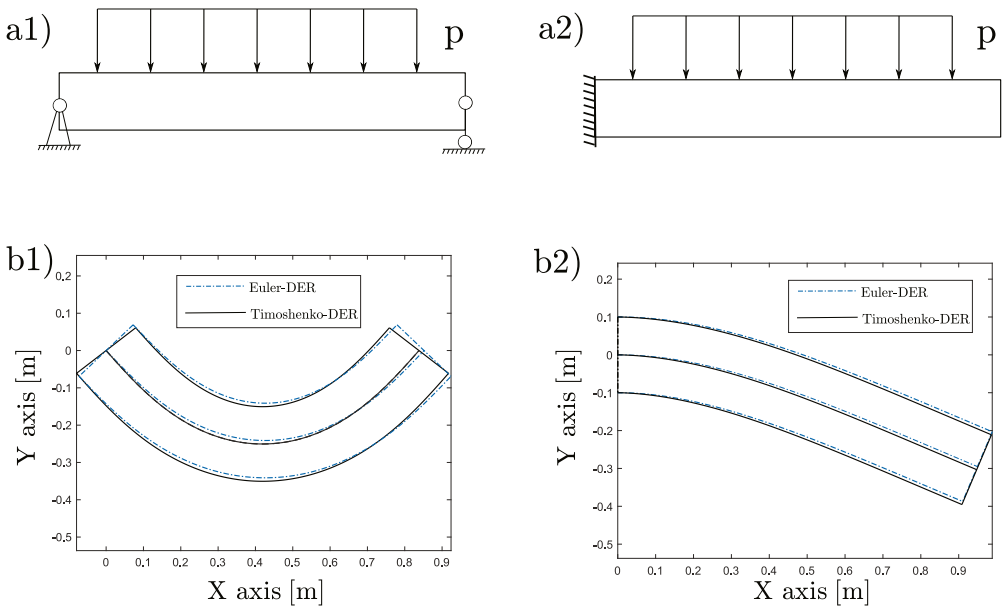

Fig. 2. Diagram of boundary and load conditions for (a1) simply supported beam and (a2) clamped-free beam. Deformed configurations of (b1) simply supported beam and (b2) clamped-free beam using Euler–Bernoulli theory and Timoshenko theory.

the constraints on the cross section are released in Timoshenko model such that its rotation makes the structure "softer".

We next systematically study the static deformations of Euler–Bernoulli beam and Timoshenko beam. In Fig. 3(a), we plot the normalized maximum deflection, w_{m}/L, (for simply supported beam, $w_{\mathrm{m}} = w(L/2)$, and for clamped-free beam, $w_{\mathrm{m}} = w(L)$), as a function of the normalized load $\bar{p} = pL^3/EI$. As expected, for the same distributed loading, the deflection of Timoshenko beam theory is always larger than the one in Euler–Bernoulli model. Also, we find a good match between analytical results and numerical data for both Euler–Bernoulli and Timoshenko beams when the structure remains in small deformation regime, i.e. $w_{\mathrm{m}}/L < 5\%$; however, as the external loading increases, the beam deforms into geometrically nonlinear phase and the analytical solution following Timoshenko model always predicts a larger value for beam deflection. This limitation for the analytical "linear" solution can be attributed to ignoring the rigidity induced by geometric nonlinearity. The simulation results, on the other hand, can successfully capture the geometrically nonlinear deformation of both Euler–Bernoulli and Timoshenko model.

In Fig. 3(b) and (c), we display the variations of beam deflection and the shear strain along its arclength, respectively, with a fixed external loading of $\bar{p} = 25.5$ for simply supported beam and $\bar{p} = 3$ for clamped-free beam. All the results indicate that the Euler theory tends to underestimate the deflection together with the rotation angle when the beam is thick, and the linear assumption tends to overestimate the deformation in geometrically nonlinear situation. A comparison between the Timoshenko-based discrete simulation and FEM results is presented in Appendix D.

3.2. Dynamic vibration and natural frequency

We now turn to the dynamic behavior of the Timoshenko beam and contrast it with the Euler–Bernoulli beam. Again, we consider the simply supported beam and clamped-free beam as examples in our analysis on natural frequency. The geometric and material properties of the beam remain unchanged from the previous example in Fig. 2. In order to initiate the vibration in beam, a small displacement is applied at $t = 0$ and subsequently released. The structure then undergoes a vibratory motion and the corresponding frequency is its natural frequency. In Fig. 4, we plot the normalized maximum deflection, w_{m}/L, in the beam as a function of time, for both simply supported beam (Fig. 4(a)) and clamped-free beam (Fig. 4(b)). Our numerical framework is symplectic and momentum preserving such that the structure can undergo a vibratory motion regardless of the time step size h [50]. This should be contrasted with artificial energy dissipation of first order backward Euler integration scheme that will lead to eventual decay of the vibration.

To understand the influence of beam thickness on the vibration, in Fig. 5(a-c), we show the relation between natural frequency, f, and the normalized beam diameter, D/L, at different ratios between Young's modulus and effective shear modulus, E/kG. The frequency in Timoshenko beam simulation matches the one achieved by standard DER framework (Euler–Bernoulli model) when the beam is thin and slender, i.e. $D/L < 0.2$. However, Euler beam model indicates that the frequency of a beam always linearly increases as a function of normalized diameter. On the other hand, Timoshenko beam simulation shows a nonlinear relation between frequency and diameter when the beam becomes thicker. The mismatch between the two models is obvious in Fig. 3(a-c) when $D/L > 0.3$. In the simply supported case, we can analytically solve the Euler–Lagrange equation for both the Euler–Bernoulli beam and Timoshenko beam, and compare the analytical solution with the simulation data. A good match between the numerical simulations and analytical results in Fig. 5(a1)–(c1) indicates the correctness of our numerical framework. Details of the analytical formulation can be found in Appendix B. Also, our results show the influence of relative shear stiffness E/kG: the larger the E/kG, the lower the frequency. The beam becomes "softer" when kG is small and the frequency is, therefore, lower. Note that $kG = \infty$ for Euler–Bernoulli beam as the shear strain and related elastic energy are neglected.

3.3. Curved beam

The simple examples discussed above with naturally straight beams can be largely understood using analytical solutions. The simulation, on the other hand, can account for arbitrary boundary conditions, external loading, and natural shapes, where analytical approach is intractable. In this section, we use a curved beam as a

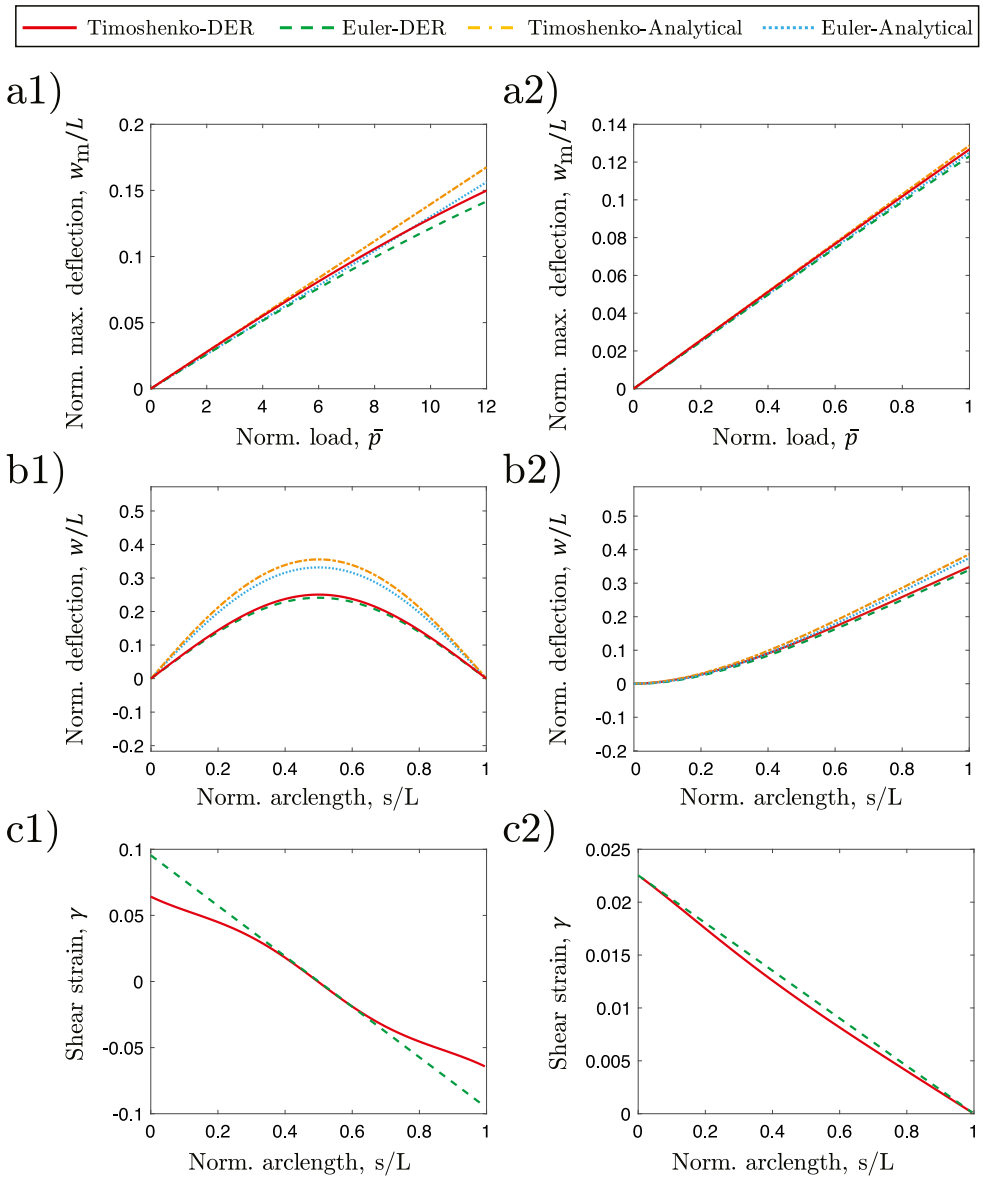

Fig. 3. For (a) a simply supported beam and (b) a clamped-free beam, (1) normalized maximum deflection, w_m/L, as a function of normalized distributed loading, $\bar{p}$; (2) normalized deflection, w/L vs. arclength; and (3) shear strain γ versus arclength.

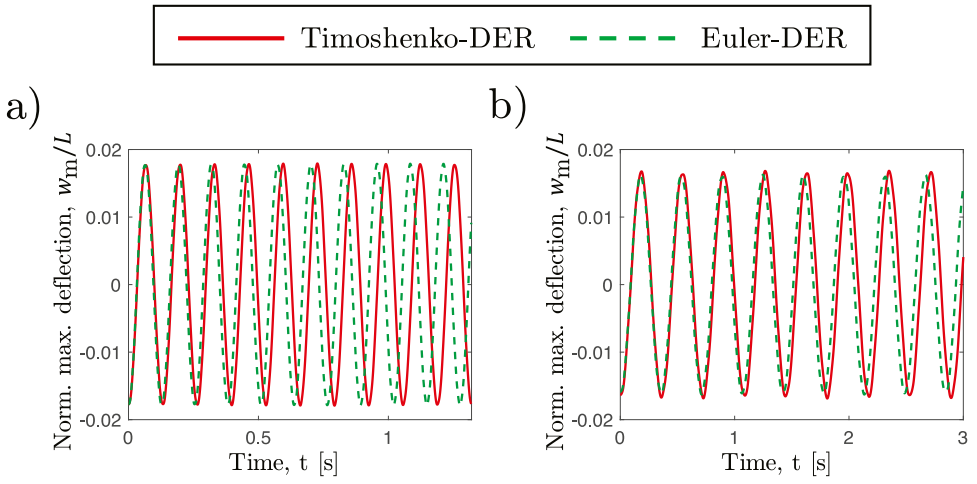

Fig. 4. Normalized maximum displacement w_m/L as a function of time for (a) simply supported beam; and (b) clamped-free beam.

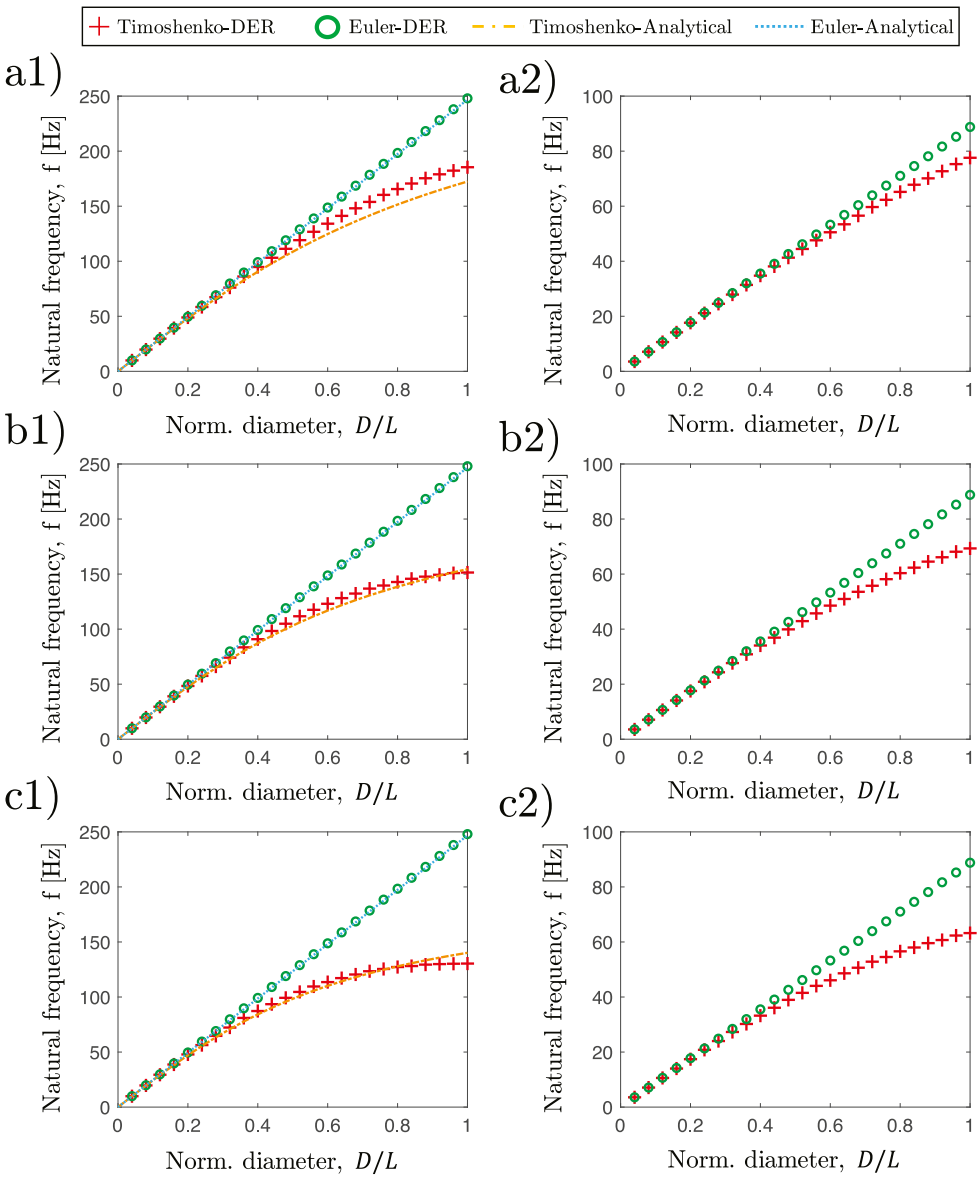

Fig. 5. Natural frequency as a function of normalized diameter, D/L, with different ratio of E/kG: (b) $E/kG = 1$; (c) $E/kG = 2$; and (d) $E/kG = 3$ for left: simply supported beam; and right: clamped-free beam.

demonstration to reveal the generality of the DDG-based simulation for Timoshenko beams. As shown in Fig. 6(a), we consider a simply supported curved beam with the following geometric and material parameters: radius of curvature $\mathbb{R} = 1.0$ m, central angle $\Theta = 120°$, Young's modulus $E = 10$ MPa, rod radius $R = 0.1$ m, and modulus' ratio $E/kG = 3$. We apply a concentrated load P at the middle point to evaluate its mechanical response.

In Fig. 6(b), we plot the load displacement relation for a curved beam, with two different numerical frameworks: standard DER method with Euler–Bernoulli model (dashed line) and Discrete Timoshenko beam method (solid line). For a fixed displacement, the external force required by Euler–Bernoulli beam is always larger than the one needed by Timoshenko theory. On the other hand, the load displacement curves show a non-monotonous trend in both the cases: the external load first increases as the deflection increases; when the midpoint goes beyond a certain value ($\Delta_{\text{mid}}/R \approx 0.3$), the external force starts to decrease as the midpoint displacement continues to increase. In other words, for a curved beam with an external load at the midpoint, two equilibrium states are possible at a fixed value of P. In Fig. 6(c1) and (c2), we illustrate the deformed shapes of the two equilibrium states under the same normalized external load $\bar{P} \equiv P\mathbb{R}^2/EI = 9.62$. However, only the configuration before the peak (in Fig. 6(c1)) is stable, while another state (in Fig. 6(c2)) is unstable. The higher rigidity of the Euler–Bernoulli beam model is also evident from Fig. 6(b): the external force required at the same midpoint displacement is always lower in case of Timoshenko beam.

4. Conclusion

We have developed a DDG-based numerical framework for geometrically nonlinear deformation of thick beam — known as Timoshenko beam, inspired by the well-established Discrete Elastic Rods (DER) method. For this purpose, we introduced the shear strain as additional degree of freedom in the standard DER method to account for the rotation of the cross section and the shear strain energy. We found that the rigidity and natural frequency of Timoshenko beam is lower than that of the Euler–Bernoulli beam, because rotation of cross section is allowed in

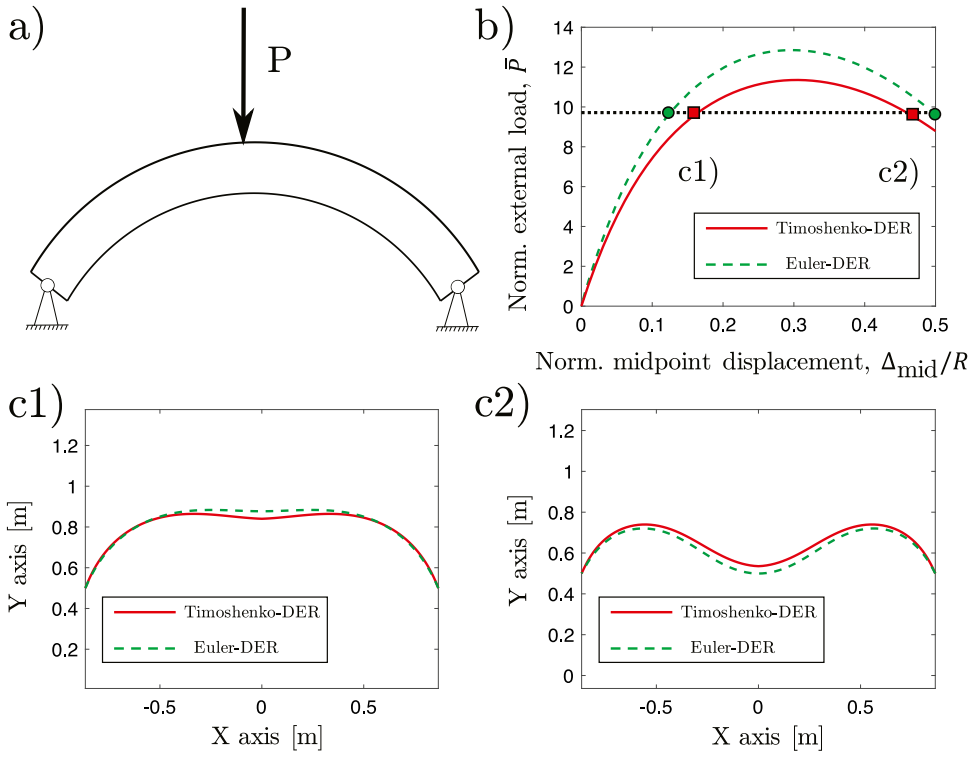

Fig. 6. (a) Diagram of the curved beam with simply supported boundary condition. (b) Plot of load versus displacement for both Euler and Timoshenko formulations. (c) Equilibrium configurations of a curved beam under a normalized external force of $\bar{P} = 9.62$: (c1) before the peak and (c2) after the peak.

Timoshenko's formulation. Moreover, we analytically solved the Euler–Lagrange equations in both Euler–Bernoulli beam and Timoshenko beam theories, and used these solutions for comparison with the numerical data obtained in our newly introduced simulator. A good match between analytical results and numerical data in linear regime indicates the correctness and accuracy of our discrete method. This framework can now robustly capture the nonlinear dynamic process of both slender and thick beams in planar case, where no twisting is involved. Future work may focus on the simulation of both shearable and extensible rod, e.g. plectoneme-solenoid transition of Cosserat rod [44,51]. We hope that the numerical tool can motivate further research in areas where thick beams are involved in geometrically nonlinear deformation, e.g. modeling of actuators in soft robotics.

Declaration of competing interest

The authors declare that they have no known competing financial interests or personal relationships that could have appeared to influence the work reported in this paper.

Acknowledgments

We are grateful for financial support from the Henry Samueli School of Engineering and Applied Science, University of California, Los Angeles.

Appendix A. Discrete formulation of bending energies

Here, we discuss the discretization process from Eqs. (2) to (5). In Fig. A.7, we discrete the rod centerline into N nodes, and the direction vector between the ith node and the $(i+1)$th node is

$$\mathbf{t}_i = \frac{\mathbf{x}_{i+1} - \mathbf{x}_i}{\|\mathbf{x}_{i+1} - \mathbf{x}_i\|}. \tag{A.1}$$

In the Discrete Elastic Rods method, the curvature between three consecutive nodes, $\{\mathbf{x}_{i-1}, \mathbf{x}_i, \mathbf{x}_{i+1}\}$, is given by,

$$\kappa_i = 2\tan(\phi_i/2)/\Delta l_i, \tag{A.2}$$

where $\phi_i = \tan^{-1}\frac{\|\mathbf{t}_{i-1}\times\mathbf{t}_i\|}{\mathbf{t}_{i-1}\cdot\mathbf{t}_i}$ is the turning angle between $\mathbf{t}_i$ and $\mathbf{t}_{i+1}$; and Δl_i is the Voronoi length associated with the ith node.

For the naturally straight beam, i.e. $\bar{\kappa} = 0$, the elastic bending energy in Eq. (5) can be re-written as

$$E_{\text{bending}} = \frac{1}{2}\frac{EI}{\Delta l_i}\sum_{i=1}^{N-2}\left[2\tan(\frac{\phi_i}{2}) + \gamma_i - \gamma_{i-1}\right]^2. \tag{A.3}$$

However, this formulation is under the assumption that the cross section is perpendicular to the rod centerline. If the angle between the normal to the centerline and the cross section at the ith node is γ_i, the angle between two consecutive material normals, $\{\mathbf{n}_{i-1}, \mathbf{n}_i\}$, at this node can be computed by (see Fig. A.7 as reference)

$$\psi_i = \phi_i + \gamma_i - \gamma_{i-1}. \tag{A.4}$$

The bending energy, instead of the turning angle between the tangential of beam centerline, $\{\mathbf{t}_{i-1}, \mathbf{t}_i\}$, is defined on the basis of the misalignment between material normals, $\{\mathbf{n}_{i-1}, \mathbf{n}_i\}$ [44,51],

$$E'_{\text{bending}} = \frac{1}{2}\frac{EI}{\Delta l_i}\sum_{i=1}^{N-2}\left[2\tan(\frac{\psi_i}{2})\right]^2. \tag{A.5}$$

In Fig. A.8, we plot the normalized maximum displacement as a functional of normalized loading, in two cases: (a) simply supported boundary conditions and (b) clamped-free boundary conditions, with different energy functionals formulated in Eqs. (A.3) and (A.5). We can clearly see that the difference between these two discrete bending energies can be neglected even in the nonlinear regime. The physical and geometric parameters here are the same as the ones used in Section 3.1.

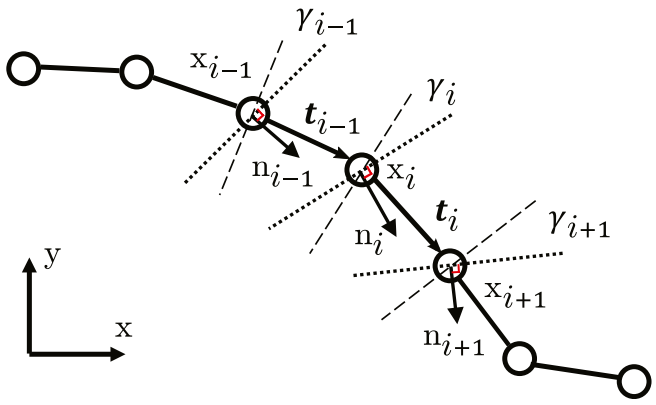

Fig. A.7. Discrete diagrams of planar rod system.

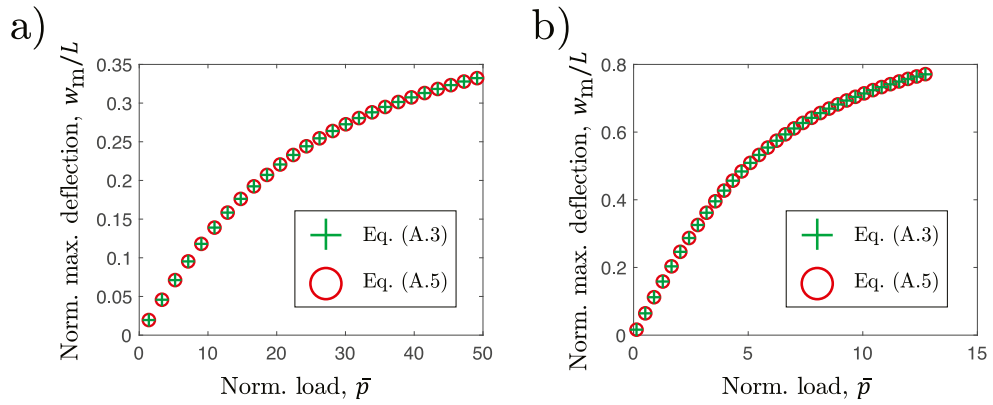

Fig. A.8. Normalized load versus normalized maximum displacement with different discrete bending energy functional in Eqs. (A.3) and (A.5) for (a) simply supported beam and (b) clamped-free beam.

Appendix B. Linear analytical solution

We review the analytical solution of both Euler–Bernoulli beam and Timoshenko beam in linear range. The main assumption in linear beam theory is

$$w' \approx \theta, \text{ and} \tag{B.1a}$$

$$w'' \approx \kappa. \tag{B.1b}$$

In addition, we ignore the axial strain, ϵ. With the assumptions mentioned above, we can write the governing equation of Euler–Bernoulli beam in static case as

$$\frac{d^2}{dx^2}\left(EI\frac{\mathrm{d}^2 w}{\mathrm{d}x^2}\right) - p = 0, \tag{B.2}$$

where p is the uniform distribution load density and w is the deflection of beam. We assume that the deflection is a fourth degree polynomial function of x, such that we can solve the polynomial coefficients on the basis of the specific boundary conditions discussed in this paper (simply supported beam and clamped-free beam; see Fig. 2(a)),

$$\text{SS}: w_{\text{Euler}} = \frac{px}{24EI}(L^3 - 2Lx^2 + x^3), \text{ and} \tag{B.3a}$$

$$\text{CF}: w_{\text{Euler}} = \frac{px^2}{24EI}(x^2 + 6L^2 - 4Lx), \tag{B.3b}$$

where L is the total length of beam. We can easily get the maximum deflection in these two cases,

$$\text{SS}: (w_{\text{m}})_{\text{Euler}} = \frac{5pL^4}{384EI}, \text{ and} \tag{B.4a}$$

$$\text{CF}: (w_{\text{m}})_{\text{Euler}} = \frac{pL^4}{8EI}. \tag{B.4b}$$

We next turn to the Timoshenko beam. The governing equation of the Timoshenko beam, similar to the Euler–Bernoulli beam, is given by

$$\frac{d^2}{dx^2}\left(EI\frac{\mathrm{d}^2 w}{\mathrm{d}x^2}\right) + \frac{EI}{kGA}\frac{\mathrm{d}^2 p}{\mathrm{d}x^2} - p = 0, \tag{B.5}$$

where k is the Timoshenko shear coefficient. We formulate the deflection of Timoshenko beam in terms of Euler solutions in Eq. (B.3): [52]

$$\text{SS}: w_{\text{Timo}} = w_{\text{Euler}} + \frac{p}{2kGA}x(L - x), \text{ and} \tag{B.6a}$$

$$\text{CF}: w_{\text{Timo}} = w_{\text{Euler}} + \frac{p}{kGA}x(L - \frac{x}{2}). \tag{B.6b}$$

The parameter γ, related to the rotation of beam cross section, follows

$$\frac{\mathrm{d}\gamma}{\mathrm{d}x} = -\frac{p}{kAG}, \tag{B.7}$$

such that γ is a linear function of x for both simply supported beam and clamped-free beams such that

$$\text{SS}: \gamma = \frac{p}{kGA}(\frac{L}{2} - x), \text{ and} \tag{B.8a}$$

$$\text{CF}: \gamma = \frac{p}{kGA}(L - x). \tag{B.8b}$$

In Fig. 2, we plot the linear analytical solutions of both Euler–Bernoulli beam and Timoshenko beam formulated above.

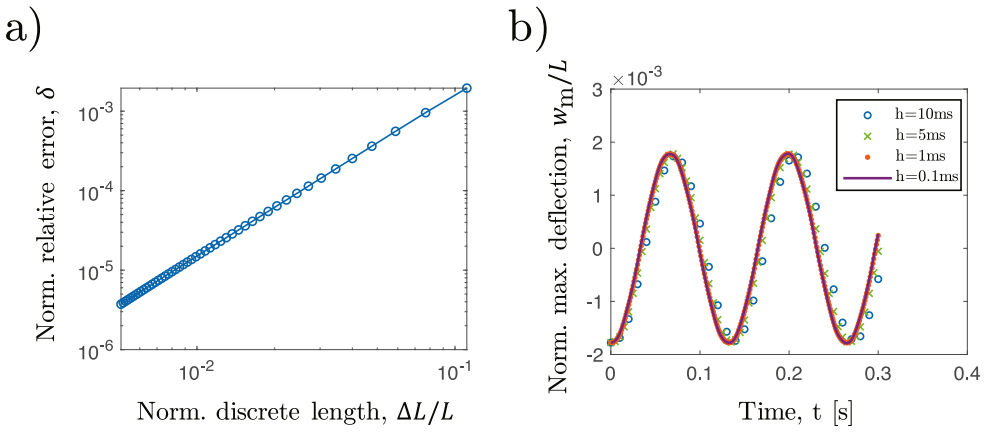

Fig. C.9. Convergence study of (a) space discretization and (b) time discretization.

For dynamic analysis, the inertial terms should be taken into account. The governing equation of Euler–Bernoulli beam, evaluated by variational principle in Eq. (3), can be written as

$$EI\frac{\partial^4 w}{\partial x^4} + \rho A\frac{\partial^2 w}{\partial t^2} = 0, \tag{B.9}$$

where ρ is the material density. For simply supported boundary condition, its deflection function can be written as

$$w(x,t) = \sin(2\pi f t)\sin(\frac{2\pi x}{L}), \tag{B.10}$$

where f is its frequency and can be evaluated from

$$f^2_{\text{Euler}} = \frac{\pi^4}{L^4}\frac{EI}{\rho A}. \tag{B.11}$$

The governing equation of Timoshenko beam can be analyzed by

$$EI\frac{\partial^4 w}{\partial x^4} + \frac{\rho^2 I}{kG}\frac{\partial^4 w}{\partial t^4} - \rho I(1+\frac{E}{kG})\frac{\partial^4 w}{\partial x^2 \partial t^2} + \rho A\frac{\partial^2 w}{\partial t^2} = 0. \tag{B.12}$$

Similarly, the estimated natural frequency of the Timoshenko beam with simply supported boundary conditions can be obtained from [53],

$$f^2_{\text{Timo}} = \frac{kG}{2\rho r^2}\left\{1 + \frac{\pi^2 r^2}{L^2}\left(1+\frac{E}{kG}\right) - \sqrt{\left[1+\frac{\pi^2 r^2}{L^2}\left(1+\frac{E}{kG}\right)\right]^2 - 4\frac{\pi^4 r^4}{L^4}\frac{E}{kG}}\right\} \tag{B.13}$$

where $r = \sqrt{\frac{I}{A}}$ is the radius of gyration of the cross section. The analytical results evaluated in Eqs. (B.11) and (B.13) for simply supported beam are shown in Fig. 5.

Appendix C. Convergence study

In this Appendix, we present a convergence study for both spatial and temporal discretization. We use the clamped-free under uniform load (Fig. 2(a2)) as the example case. In Fig. C.9(a), we plot the normalized error, $\delta = (w_m - \bar{w}_m)/\bar{w}_m$, as a function of normalized discrete edge length, $\Delta L/L$, for clamped-free beam, where w_m is the maximum deflection of the beam and $\bar{w}_m$ is the maximum deflection in the "exact" case. The "exact" solution, $\bar{w}_m$, is obtained with $\Delta L = 10^{-3}$ m, i.e. number of nodes, $N = 1000$. The material and geometric parameters are the same as the ones used in Section 3: rod length $L = 1.0$ m, circular radius, $R = 0.1$ m, Young's modulus $E = 10$ MPa, and Poisson ratio $\nu = 1/8$.

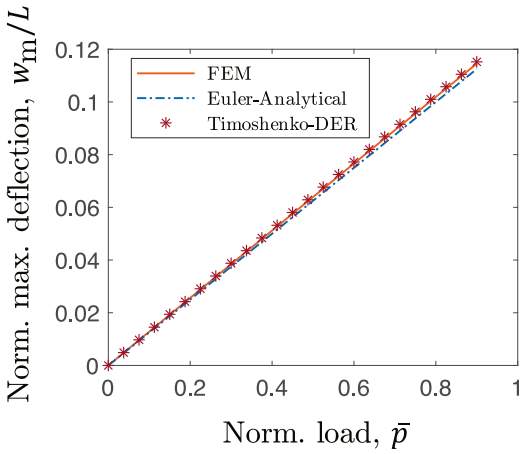

Fig. D.10. Normalized maximum displacement as a function of normalized load, from Finite Element Analysis, Discrete Timoshenko beam simulation, and Euler–Bernoulli beam theory.

The numerical results show quadratic convergence with space discretization.

In Fig. C.9(b), the maximum deflection in the beam as a function of time is plotted at different values of time step size ranging from $h = 10$ ms to $h = 0.1$ ms. We find negligible variation in the time series of the deformation as long as $h \lesssim 5$ ms.

Appendix D. Comparison with finite element method

In this Appendix, we compare our reduced model with Finite Element Method (FEM). We take a clamped-free beam with square cross section (1.0 m × 0.2 m ×0.2 m) as the example case. We used the commercial software Abaqus/Standard for our static FEM simulations. We modeled the beam as a linear elastic material with 8-node linear brick, incompatible modes (Abaqus type C3D8I). 40000 cube elements (100 × 20 × 20) are used in the model. The Young's modulus is $E = 10$ MPa and the Poisson ratio is $\nu = 0.3$. We choose Timoshenko shear correction $k = 5/6$ for square cross section. In Fig. D.10, we plot the load–displacement curves for clamped-free beam from three approaches: FEM analysis, analytical formulation of Euler–Bernoulli beam, and the newly introduced discrete model. A good match between 3D FEM analysis and discrete Timoshenko beam model indicates the correctness of our numerical framework. Also note that the under-prediction of deflection in Euler–Bernoulli beam analysis can be clearly observed in this figure.

References

[1] J. Wycech, Lightweight composite beam, US Patent 4,901,500, Feb. 20 1990.
[2] M. Karama, K. Afaq, S. Mistou, Mechanical behaviour of laminated composite beam by the new multi-layered laminated composite structures model with transverse shear stress continuity, Int. J. Solids Struct. 40 (6) (2003) 1525–1546.
[3] A. Tounsi, M.S.A. Houari, S. Benyoucef, et al., A refined trigonometric shear deformation theory for thermoelastic bending of functionally graded sandwich plates, Aerosp. Sci. Technol. 24 (1) (2013) 209–220.
[4] J. Pei, F. Tian, T. Thundat, Glucose biosensor based on the microcantilever, Anal. Chem. 76 (2) (2004) 292–297.
[5] N.A. Hall, M. Okandan, F. Degertekin, Surface and bulk-silicon-micromachined optical displacement sensor fabricated with the SwIFT-Lite process, J. Microelectromech. Syst. 15 (4) (2006) 770–776.
[6] W. Faris, A.H. Nayfeh, Mechanical response of a capacitive microsensor under thermal load, Commun. Nonlinear Sci. Numer. Simul. 12 (5) (2007) 776–783.
[7] Y. Moser, M.A. Gijs, Miniaturized flexible temperature sensor, J. Microelectromech. Syst. 16 (6) (2007) 1349–1354.
[8] E.S. Hung, S.D. Senturia, Extending the travel range of analog-tuned electrostatic actuators, J. Microelectromech. Syst. 8 (4) (1999) 497–505.
[9] M.P. de Boer, D.L. Luck, W.R. Ashurst, R. Maboudian, A.D. Corwin, J.A. Walraven, J.M. Redmond, High-performance surface-micromachined inchworm actuator, J. Microelectromech. Syst. 13 (1) (2004) 63–74.
[10] J.W.S.B. Rayleigh, Scientific Papers: 1869–1881, Vol. 1, University Press, 1899.
[11] S.P. Timoshenko, LXVI. On the correction for shear of the differential equation for transverse vibrations of prismatic bars, Lond. Edinburgh Dublin Phil. Mag. J. Sci. 41 (245) (1921) 744–746.
[12] S.P. Timoshenko, X. On the transverse vibrations of bars of uniform cross-section, Lond. Edinburgh Dublin Phil. Mag. J. Sci. 43 (253) (1922) 125–131.
[13] S.M. Han, H. Benaroya, T. Wei, Dynamics of transversely vibrating beams using four engineering theories, J. Sound Vib. 225 (5) (1999) 935–988.
[14] A. Labuschagne, N.J. van Rensburg, A. Van der Merwe, Comparison of linear beam theories, Math. Comput. Modelling 49 (1–2) (2009) 20–30.
[15] D. Thomas, J. Wilson, R. Wilson, Timoshenko beam finite elements, J. Sound Vib. 31 (3) (1973) 315–330.
[16] H. Nelson, A finite rotating shaft element using Timoshenko beam theory, J. Mech. Des. 102 (4) (1980) 793–803.
[17] A. Tessler, S. Dong, On a hierarchy of conforming Timoshenko beam elements, Comput. Struct. 14 (3–4) (1981) 335–344.
[18] Z. Friedman, J.B. Kosmatka, An improved two-node Timoshenko beam finite element, Comput. Struct. 47 (3) (1993) 473–481.
[19] J. Carrer, S. Fleischfresser, L. Garcia, W. Mansur, Dynamic analysis of Timoshenko beams by the boundary element method, Eng. Anal. Bound. Elem. 37 (12) (2013) 1602–1616.
[20] I. Eshraghi, S. Dag, Domain-boundary element method for elastodynamics of functionally graded Timoshenko beams, Comput. Struct. 195 (2018) 113–125.
[21] R. Scuciato, J. Carrer, W. Mansur, Dynamic analysis of Euler–Bernoulli beams by the time-dependent boundary element method formulation, Eng. Anal. Bound. Elem. 63 (2016) 134–153.
[22] R. Rodríguez, A. Galvis, P. Sollero, C.-L. Tan, E. Albuquerque, Transient dynamic analysis of generally anisotropic materials using the boundary element method, Acta Mech. 229 (4) (2018) 1893–1910.
[23] P.K. Banerjee, R. Butterfield, Boundary Element Methods in Engineering Science, Vol. 17, McGraw-Hill London, 1981.
[24] G. Chen, J. Zhou, Boundary element methods, Vol. 92, Academic Press London, 1992.
[25] E. Grinspun, M. Desbrun, K. Polthier, P. Schröder, A. Stern, Discrete differential geometry: an applied introduction, ACM SIGGRAPH Course 7 (2006) 1–139.
[26] J. Spillmann, M. Teschner, An adaptive contact model for the robust simulation of knots, in: Computer Graphics Forum, Vol. 27, 2008, pp. 497–506.
[27] M. Bergou, M. Wardetzky, S. Robinson, B. Audoly, E. Grinspun, Discrete elastic rods, ACM Trans. Graph. 27 (3) (2008) 63.
[28] M. Bergou, B. Audoly, E. Vouga, M. Wardetzky, E. Grinspun, Discrete viscous threads, in: ACM Transactions on Graphics, Vol. 29, ACM, 2010, p. 116.
[29] B. Audoly, Y. Pomeau, Elasticity and Geometry: From Hair Curls to the Non-Linear Response of Shells, Oxford University Press, 2010.
[30] Z. Shen, J. Huang, W. Chen, H. Bao, Geometrically exact simulation of inextensible ribbon, in: Computer Graphics Forum, Vol. 34, Wiley Online Library, 2015, pp. 145–154.
[31] B. Audoly, N. Clauvelin, P.-T. Brun, M. Bergou, E. Grinspun, M. Wardetzky, A discrete geometric approach for simulating the dynamics of thin viscous threads, J. Comput. Phys. 253 (2013) 18–49.
[32] D. Baraff, A. Witkin, Large steps in cloth simulation, in: Proceedings of the 25th Annual Conference on Computer Graphics and Interactive Techniques, ACM, 1998, pp. 43–54.
[33] E. Grinspun, A.N. Hirani, M. Desbrun, P. Schröder, Discrete shells, in: Proceedings of the 2003 ACM SIGGRAPH/Eurographics Symposium on Computer Animation, Eurographics Association, 2003, pp. 62–67.
[34] C. Batty, A. Uribe, B. Audoly, E. Grinspun, Discrete viscous sheets, ACM Trans. Graph. 31 (4) (2012) 113.
[35] J. Spillmann, M. Teschner, Cosserat nets, IEEE Trans. Vis. Comput. Graphics 15 (2) (2008) 325–338.
[36] J. Pérez, B. Thomaszewski, S. Coros, B. Bickel, J.A. Canabal, R. Sumner, M.A. Otaduy, Design and fabrication of flexible rod meshes, ACM Trans. Graph. 34 (4) (2015) 138.
[37] J. Panetta, M. Konaković-Luković, F. Isvoranu, E. Bouleau, M. Pauly, X-shells: A new class of deployable beam structures, ACM Trans. Graph. 38 (4) (2019) 83.
[38] M.K. Jawed, A. Novelia, O.M. O'Reilly, A Primer on the Kinematics of Discrete Elastic Rods, Springer, 2018.
[39] M.K. Jawed, F. Da, J. Joo, E. Grinspun, P.M. Reis, Coiling of elastic rods on rigid substrates, Proc. Natl. Acad. Sci. 111 (41) (2014) 14663–14668.
[40] M.K. Jawed, N. Khouri, F. Da, E. Grinspun, P.M. Reis, Propulsion and instability of a flexible helical rod rotating in a viscous fluid, Phys. Rev. Lett. 115 (16) (2015) 168101.
[41] M. Jawed, P.M. Reis, Dynamics of a flexible helical filament rotating in a viscous fluid near a rigid boundary, Phys. Rev. Fluids 2 (3) (2017) 034101.
[42] C. Baek, A.O. Sageman-Furnas, M.K. Jawed, P.M. Reis, Form finding in elastic gridshells, Proc. Natl. Acad. Sci. 115 (1) (2018) 75–80.
[43] G. Kirchhoff, Ueber das Gleichgewicht und die Bewegung eines unendlich dünnen elastischen Stabes, J. Reine Angew. Math. 56 (1859) 285–313.
[44] M. Gazzola, L. Dudte, A. McCormick, L. Mahadevan, Forward and inverse problems in the mechanics of soft filaments, R. Soc. Open Sci. 5 (6) (2018) 171628.
[45] R. Nazemnezhad, H. Shokrollahi, S. Hosseini-Hashemi, Sandwich beam model for free vibration analysis of bilayer graphene nanoribbons with interlayer shear effect, J. Appl. Phys. 115 (17) (2014) 174303.
[46] S. Kim, C. Laschi, B. Trimmer, Soft robotics: a bioinspired evolution in robotics, Trends Biotechnol. 31 (5) (2013) 287–294.
[47] K.-I. Jang, K. Li, H.U. Chung, S. Xu, H.N. Jung, Y. Yang, J.W. Kwak, H.H. Jung, J. Song, C. Yang, et al., Self-assembled three dimensional network designs for soft electronics, Nature Commun. 8 (2017) 15894.
[48] X. Zhang, F.K. Chan, T. Parthasarathy, M. Gazzola, Modeling and simulation of complex dynamic musculoskeletal architectures, Nature Commun. 10 (1) (2019) 1–12.
[49] D. Chen, D.I. Levin, W. Matusik, D.M. Kaufman, Dynamics-aware numerical coarsening for fabrication design, ACM Trans. Graph. 36 (4) (2017) 84.
[50] W. Huang, M.K. Jawed, Newmark-beta method in discrete elastic rods algorithm to avoid energy dissipation, J. Appl. Mech. 86 (8) (2019) 084501.
[51] N. Charles, M. Gazzola, L. Mahadevan, Topology, geometry and mechanics of strongly stretched and twisted filaments, 2019, arXiv preprint arXiv:1905.00796.
[52] C.M. Wang, Timoshenko beam-bending solutions in terms of Euler-Bernoulli solutions, J. Eng. Mech. 121 (6) (1995) 763–765.
[53] S.R. Singiresu, et al., Mechanical Vibrations, Addison Wesley, 1995, p. 737.